Contents lists available at ScienceDirect

Scientific African

journal homepage: www.elsevier.com/locate/sciaf

Physical Sciences

Optical modelling of TCO based FTO/TiO$_2$ multilayer thin films and simulation in hydrogenated amorphous silicon solar cell

Wycliffe M. Isoe [a,d,*], Maxwell J. Mageto [a,d], Christopher M. Maghanga [b,d], Maurice M. Mwamburi [c,d], Benjamin V. Odari [a,d]

[a] Department of Physics, Masinde Muliro University of Science and Technology, P.O. Box 190 Kakamega, Kenya
[b] Department of Physical & Biological Sciences, P.O. Box Private Bag Kabarak, Nakuru, Kenya
[c] Department of Physics, University of Eldoret, P.O. Box 1125 Eldoret, Kenya
[d] Materials Research Society of Kenya, P.O. Box 15653-00503 Nairobi, Kenya

A R T I C L E   I N F O

A B S T R A C T

Hydrogenated Amorphous silicon (a:Si:H) has low amounts of defects making it attractive for photovoltaic applications. To improve power conversion efficiency (PCE) of a:Si:H solar cells, this study investigated the effect of introducing FTO/TiO$_2$ multilayer thin films into its structure to serve as antireflection coating. The multilayer thin films were characterized and optimized by optical simulations using a computer program, GLSIM (glazing simulator). The program was written in FORTRAN and implemented in MATLAB. The multi-Fresnel equations were employed to create the GLSIM program. Then using the program, together with the pairs of real and imaginary values of complex refractive index, n and k respectively, the transmittance and reflectance data of FTO/TiO$_2$ multilayer thin films on glass substrate were computed. The optimized FTO/TiO$_2$ multilayer thin films were then incorporated into silicon solar cell with structure glass/FTO/TiO$_2$/n-a-Si:H/i-a-Si:H/p-a:Si:H/P^+-BSF and characterized using SCAPS-1D software. The effect of varying layer thickness on the solar cell performance was also investigated. The optimized solar cell had a thickness of 100 nm, 50 nm, 900 nm, 100 nm, 10μm and 5μm for FTO, TiO$_2$, n-a-Si:H, i-a-Si:H, p-a-Si:H and P^+-BSF respectively. The device output performance were 37.96 mA/cm^2, 1.34 V, 56.37% and 28.72% for Jsc, Voc, FF and η respectively showing a remarkable improvement in the solar cell performance. These results show potential of fabricating an improved hydrogenated silicon solar cell.

Introduction

The demand for energy is on an increasing trend due to the increase in population and rapid growth of global economy. This ever-increasing demand has necessitated the need for a clean, renewable and sustainable alternative source of energy. Solar energy has for a long time been considered among the best alternatives owing to its abundance but harvesting and

* Corresponding author.
  E-mail address: isoewycliffe@gmail.com (W.M. Isoe).
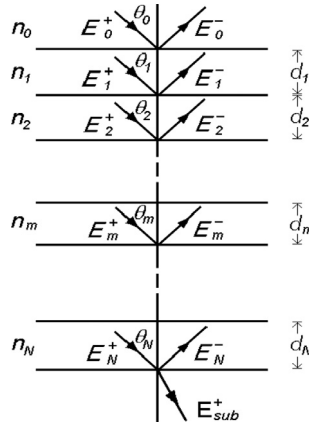
Fig. 1. Schematic illustration on how light travels through multilayer thin films. (For interpretation of the references to color in this figure legend, the reader is referred to the web version of this article.)

conversion technology has been the limiting factor. Solar cell devices are extensively employed to convert solar radiations directly to electricity.

Hydrogenated amorphous silicon based solar cells have received special attention due to their high stability and high conversion efficiencies [1]. The first time amorphous silicon solar cell was reported was in the year 1980's [2] and later on heterojunction silicon solar cells (HIT) were invented by Sanyo which showed high efficiency of 20.7%. It was discovered that intrinsic buffer layer, back surface field (BSF) and transparent conducting oxide (TCO) enhanced the performance of these silicon heterojunction solar cells [3].

Silicon solar cells have been employed for decades to convert the solar radiation to electricity. The major hindrances to achieving high efficiencies in these solar cells are losses due to unwanted reflection [4], resistivity [5], electron-hole recombination [6] as well as thermal losses [7]. Among these losses, optical losses account to about 30% [8]. It has been reported that applying antireflection coatings to the solar cells can lead to increase in transmittance of incident photons [9]. Moreover, introduction of extra elements in the TCO lattice is helpful as this leads to a reduced refractive index of the material and thus leading to the creation of an index-matched material for the glass/TCO interface [10]. Therefore, the present study presents a way of overcoming these unwanted reflections by introducing FTO/TiO$_2$ multilayer thin films to be employed as antireflective coatings on top of a silicon heterojunction solar cell.

The multilayer thin films exhibit spectrally selective transmission and reflection characteristics since they only allow peculiarly selected portions of the light spectrum to pass through while blocking some i.e., their transmission and/or reflection properties are regulated for selected and controlled packages of thermal radiation fluxes [11]. The FTO/TiO$_2$ multilayer thin films will improve light trapping mechanism while at the same time, the incorporated TiO$_2$ will improve transmissivity of the multilayer thin films.

The optimized FTO/TiO$_2$ multilayer thin films were then incorporated on silicon n-i-p solar cell and characterized using SCAPS-1D software [12]. The obtained data were employed to analyse the solar cell output performance i.e., short circuit current density (Jsc), cell conversion efficiency (η), open circuit voltage (Voc), and fill factor (FF).

Numerical model for FTO/TiO2 multilayer thin films and material parameters

When light strikes the interface between two optically different materials, some light is reflected while some passes through, as illustrated in Fig. 1. If the medium on what is arbitrarily taken to be the outward (o) of the interface has a complex refractive index n'_o and the medium on the inside (i) has refractive index n'_i, then, for a given wavelength, Snell's law is stated as shown in Equation (1) [13]

$$n'_o \sin(\theta_o) = n'_i \sin(\theta_i) \tag{1}$$

Where θ_o and θ_i are angles of incidence and refraction respectively.

For an incident wave of amplitude ε_o^+ travelling through the interface from outside to inside, the amplitude reflection coefficient *(r)* and transmission coefficient *(t)* are defined as shown in Equation (2).

$$r_{oi} = \frac{\varepsilon_o^-}{\varepsilon_o^+} t_{oi} = \frac{\varepsilon_i^+}{\varepsilon_o^+} \tag{2}$$

Where ε_o^- and ε_i^+ are the amplitudes of the reflected and transmitted waves. For waves travelling in opposite direction, the same expressions will hold for which it can be demonstrated that:

$$r_{io} = -r_{io} t_{io} t_{io} - r_{io} r_{io} = 1 \tag{3}$$

Where r_{io} and t_{io} are total reflection and to transmittance Fresnel amplitudes respectively. The minus (-n) sign in the subscript shows the direction of the incident light on the interface.

The reflectance (ρ) and transmittance (τ) of an interface are defined in terms of incident, reflected and transmitted beam intensities (*i*) as shown in Equation (4).

$$\rho_{oi} = \frac{I_0^-}{I_o^+} \tau_{oi} = \frac{I_i^+}{I_o^+} \tag{4}$$

Plane-polarized radiation can be regarded as the superposition of two orthogonal plane-polarized waves with zero phase difference, one with the electric field normal to the plane of incidence (p-polarization).

The physical laws governing the reflection and transmission of radiation at an interface are different for each polarization and are given by the following Fresnel equations standardized in DIN 1349 (1972) [14].

$$r_{oi}^s = \frac{n'_o \cos(\theta_o) - n'_i \cos(\theta_i)}{n'_o \cos(\theta_o) + n'_i \cos(\theta_i)} t_{oi}^s = \frac{2n'_o \cos(\theta_o)}{n'_o \cos(\theta_o) + n'_i \cos(\theta_i)}$$
$$r_{oi}^p = \frac{n'_o \cos(\theta_o) - n'_i \cos(\theta_i)}{n'_o \cos(\theta_o) + n'_i \cos(\theta_i)} t_{oi}^P = \frac{2n'_o \cos(\theta_o)}{n'_o \cos(\theta_o) + n'_i \cos(\theta_i)} \tag{5}$$

It can be demonstrated that;

$$\rho^s = (r^s)^2 \rho^p = (r^p)^2$$
$$\tau^s = (\tau^s)^2 \tau^p = (\tau^p)^2 \tag{6}$$

When computing the radiation transfer of multilayer systems, the total reflectance of the system (ρ^T) is calculated by averaging all the reflectances obtained from the two sets of polarized radiation. The total transmittance (τ^T) is obtained in a similar way by finding the mean of the two polarized transmittances.

Now in modelling optically the properties of TCO based FTO/TiO$_2$ multilayer thin films on a glass substrate, the transfer of radiation through both coherent and incoherent layers are considered. Also, the impacts of interference and absorption are considered. These make it possible for the total reflectance and total transmittance of whatsoever combination of thin and thick layers to be established. Here, the term *total* is employed to mean the net reflectance and transmittance of all combined layers in a stack.

The calculations employ a matrix multiplication approach in which the effect on radiation of each interface and of each layer is represented by individual matrices. The interface matrix stands for the relation between the amplitudes or intensities of the radiation fields on each side of the interface between two layers. On the other hand, the layer matrix defines the attenuation of the radiation as it travels through a layer.

A function to calculate reflectance and transmittance for a stack of thin (coherent) and thick (non-coherent) with known complex indices of refraction, N was created and implemented in MATLAB. The complex indices of refraction were obtained from literature [15,16]. The code is shown in Appendix 1. The calculation uses the matrix formalism described by P Pfrommer et al. [17] together with equations described in section 1.1 above. Thick and thin layers can be mixed in arbitrary order, and the number of layers is limited only by the memory and speed of your computer but a thick layer must be thick for all wavelengths. In this simulation, a 1 mm thick glass was assumed as the incoherent layer while FTO and TiO2 layers were assumed as coherent. The wavelength was interpolated to lambda step length. The computer GLSIM program made it possible to vary the film thicknesses in an endeavour to find the optimum thicknesses for the films.

Device simulation of hydrogenated amorphous silicon solar cell with the structure **glass/FTO/TiO$_2$/n-a-Si:**
H/i-a-Si:H/p-a-Si:H/p$^+$-BSF

The designing and characterizing of silicon solar cell were done using SCAPS-1D (Solar Cell Capacitance Simulator One dimension) version 3.3.07 ("SCAPS3307") simulation tool [12]. The SCAPS-1D software has the ability to solve the fundamental semiconductor equations; the Poisson equations, the continuity equations for electrons and holes and carrier transport [18]. The working point conditions of the SCAPS-1D simulations were temperature 300 K, work point bias voltage 0 V and frequency of $1.0 \times$ '10$^6 Hz$. The simulation was done under AM1.5 G 1 sun spec.

The solar cell structure consists of FTO /TiO$_2$ multilayer thin films, n-a-Si:H buffer layer, i-a-Si:H emitter layer, p-a-Si:H absorber layer, and p^+-BSF back surface field layer as shown in Fig. 2. FTO/TiO$_2$ multilayer thin films are employed as transparent conducting oxide (TCO), antireflection coatings as well as front electrode.

The layer parameters employed in the simulation were extracted from literature [19–23], and summarized in Table 1. The device output performance was majorly based on the electrical, optical, material, and device parameters used in the simulation.

Results and discussion

Optical studies of FTO/TiO$_2$ multilayer thin films

Fig. 3 shows the optical transmittance and reflectance for various FTO and TiO$_2$ thicknesses in the wavelength range 300 nm-2500 nm.
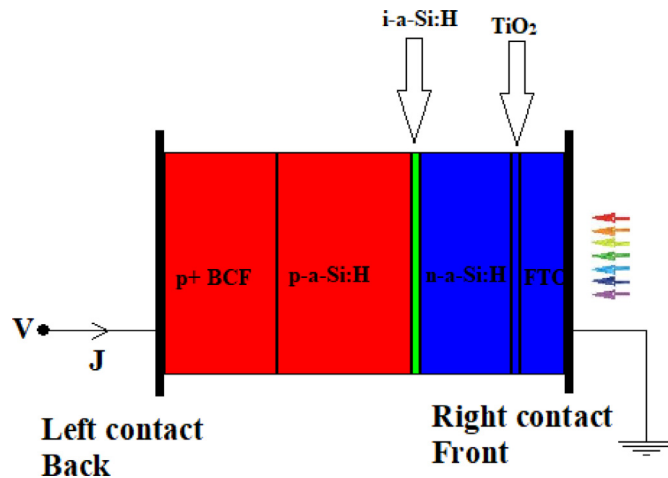
Fig. 2. Silicon solar cell model. (For interpretation of the references to color in this figure legend, the reader is referred to the web version of this article.)

Table 1
Layer parameters used for simulation silicon solar cell.

Solar cell parameter	FTO	TiO$_2$	n-a-Si:H	i-a-Si:H	p-a-Si:H	p^+-BSF
Band gap,E_g (eV)	3.6	3.26	1.74	1.72	1.12	1.72
Thickness, t (μm)	0.2	0.05	0.05	0.05	10	5
Electron affinity, χ_e (eV)	4	4.26	3.9	3.9	4.05	4.05
Relative Dielectric permittivity, ε_r.	9	10	11.9	11.9	11.9	11.9
N$_C$ effective density(cm-3)	$2.2 \times '10^{18}$	$2.2 \times '10^{18}$	$1.0 \times '10^{20}$	$1.0 \times '10^{20}$	2.8×10^{19}	2.8×10^{19}
N$_D$ effective density(cm^{-3})	$1.8 \times '10^{19}$	$1.8 \times '10^{19}$	$1.0 \times '10^{20}$	$1.0 \times '10^{20}$	$1.04 \times '10^{19}$	$1.04 \times '10^{19}$
Electron thermal velocity (cm/s)	$1.0 \times '10^7$	$1.0 \times '10^7$	$1.0 \times '10^7$	$1.0 \times '10^7$	$1.0 \times '10^7$	$1.0 \times '10^7$
Hole thermal velocity (cm/s)	$1.0 \times '10^7$	$1.0 \times '10^7$	$1.0 \times '10^7$	$1.0 \times '10^7$	$1.0 \times '10^7$	$1.0 \times '10^7$
Electron mobility,μ_n (cm2/Vs)	20	20	20	20	20	20
Hole mobility, μ_p (cm^2/Vs)	10	10	5	5	5	5
Carrier density of the donor, N$_D$ (cm^{-3})	1.0×10^{18}	5.0×10^{17}	1.0×10^{20}	0	0	0
Carrier density of the acceptor, N$_A$ (cm^{-3})	0	0	0	0	1.5×10^{19}	1.0×10^{20}

The spectra data that were used to draw the graphs in origin software were obtained from MATLAB simulation. The different film thicknesses shown were meant to determine which film thickness combinations would give optimum visible transmittance. All the film combinations exhibit high transmittance and low reflectance in the visible range. However, it was observed that transmittance decreased with increase in TiO$_2$ thickness in the visible wavelength range whereas the reflectance increased with wavelength in the near infrared (NIR) region. This is because as TiO$_2$ thickness increases, more bound electrons are available for excitation causing a reduction in transmittance as observed.

The high reflectance at NIR regions may also be associated with large number of free carriers present due to increased film thicknesses. This high transmittance as well as high reflectance in the NIR region and low absorption in the visible wavelength range affect plasmon absorption onset. This observed behaviour of the multilayer thin films in the visible and NIR regions are the desired material properties of a well performing anti-reflective coating for solar cell applications [24]. Further, the reduction of transmittance and the rise of reflectance at NIR region is an indicator that the films are good electrical conductors [25].

Also, it is observed that the peak of the transmittance and reflectance curves shift with increase in wavelength for different thicknesses in both 3a and 3b. The shifts in the transmittance and reflectance fringes suggests that the films are morphologically homogeneous [26]. The crossing over of T and R at different wavelengths as observed in 3(b), 3(c) and 3(d) show the position of the plasma wavelength, ω_p. The plasma frequency is employed to characterize the reflection by the free carriers.

From the analysis of the results, it was observed that the best multilayer films combination is FTO (100 nm)/TiO$_2$(5 nm) multilayer thin films which have average transmittance and reflectance of 0.82 and 0.33 respectively in 380 nm-780 nm wavelength range.

Fig. 4 shows the absorption spectra of the optimum multilayer thin films combination i.e., FTO (100 nm)/TiO$_2$ (5 nm). It is observed from Fig. 4 that the absorption reduces with increase in wavelength before it starts to raise again at around 888 nm
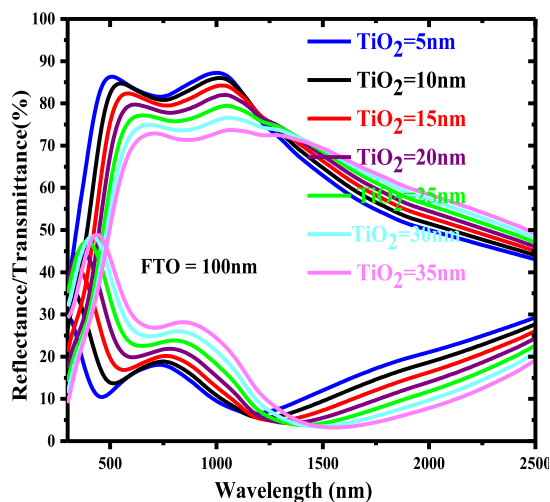
(a)
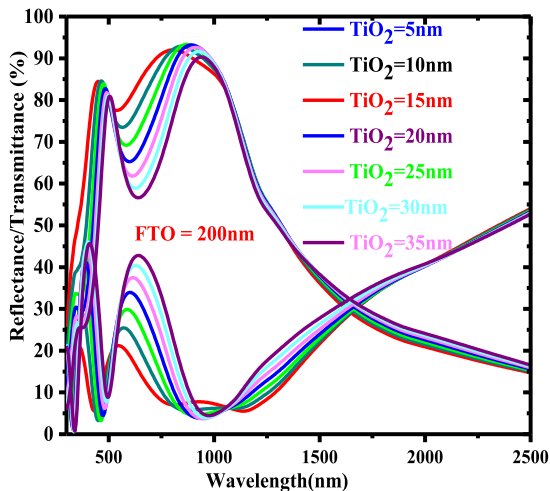
(b)
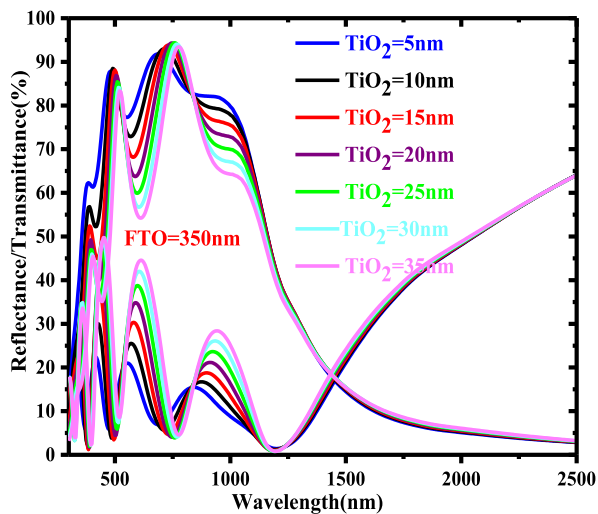
(c)
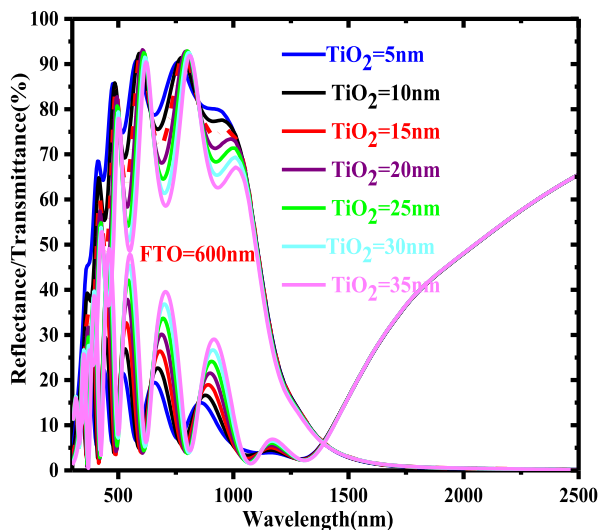
(d)

Fig. 3. Reflectance and transmittance spectra of FTO/TiO$_2$ multilayer films on glass substrate for (a) FTO (100 nm), (b) FTO (200 nm) (c) FTO (350 nm) and (d) FTO (600 nm) for various TiO$_2$ film thicknesses. (For interpretation of the references to color in this figure legend, the reader is referred to the web version of this article.)

wavelength. The absorption in the region 543 nm-888 nm wavelength range is almost zero meaning that at this region, the transmittance is very high and the films have very low reflectance. Therefore, the reflectance losses are minimized with this multilayer combination since most reflectance losses occur within 600 nm-900 nm wavelength range [27].

Optical losses greatly affect the power from a solar cell by lowering the short-circuit current. Optical losses are made up of radiations, which otherwise could have generated an electron – hole pair. Anti-reflection coatings on the top surface of the solar cell is one of the many ways of reducing these losses. Thus, the optimized FTO/TiO$_2$ coating will greatly minimize these losses. .
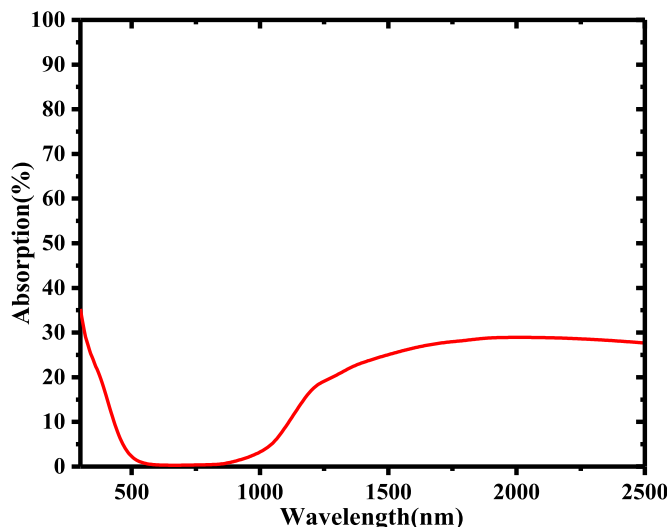
Fig. 4. Spectral absorptance $A = 1-(R + T)$ for the FTO (100 nm)/TiO2(5 nm) multilayer thin films combination. (For interpretation of the references to color in this figure legend, the reader is referred to the web version of this article.)

Numerical study of n-i-p based amorphous hydrogenated solar cell using SCAPS-1D device simulation

Effect of n-a-Si:H thickness

Fig. 5 show the effect of varying n-a-Si:H layer thickness on the solar cell performance. It is observed that the performance of the solar cell is greatly influenced by the variation of the layer thickness. Fig. 5(a), 5(b), 5(c) and 5(d) demonstrate that when the layer thickness is varied from 100 nm to 1500 nm, the values of the solar cell output parameters i.e. FF, η, V_{oc} and J_{sc} also varies. The optimum efficiency of 28.74% is obtained with a layer thickness of 900 nm. The values of FF, η, and J_{sc} increases with increase of the layer thickness to a maximum value while that of V_{oc} decreases with increase of layer thickness..

The values FF, η, and J_{sc} start to slightly decrease after a thickness of 900 nm. This majorly is because, with increased n-a-Si:H later thickness, the generated charge carriers recombine before reaching the electrodes at the surface. Also, the diffusion length depends on the average time between the creation of the charge carrier and the recombination in a material. It is evident that the smaller thickness of n-a-Si:H increases the lifetime of the charge carriers. This longer time is required to facilitate the electron-hole pairs to reach the surface as well as yielding sufficient amount of photocurrent. Thus, a n-a-Si:H thickness of less than 1000 nm will allow absorbed photons to reach the absorber layer as well minimize the rate of recombination. Other layer thicknesses were also optimized and it was found out that thicknesses of 100 nm, 50 nm, 100 nm, 10μm and 5μm for FTO, TiO2, i-a-Si:H, p-a-Si:H and P^+-BSF respectively gave optimum solar cell performance. This is well explained in our other similar published work [28].

With these optimum layer thicknesses, a J-V characteristics curve was computed and the result is presented in Fig. 6. Solar cell parameters deduced from this curve are also presented. The solar cell parameters indicate an improved solar cell performance with a power conversion efficiency of 28.74%

Capacitance and conductance of FTO/TiO$_2$/n-a-Si:H/ i-a-Si:H/ p-a-Si:H/p$^+$-BSF silicon solar cell

Fig. 7 shows the simulated c-v curves of the silicon solar cell under illumination. It has been found that the simulated capacitance and conductance increases with voltage. The shape of the curves is in agreement with Crandall's equation for photo-capacitance, shown in Equation (7) [3].

$$C_{ph} = \frac{qGd^3}{2(\mu_p + \mu_n)(V_{BI} - V)^2} \tag{7}$$

where G is the generation rate, d is the sample thickness, V_{BI} is the built-in voltage, V is the applied dc bias voltage, μ_p and μ_n are hole and electron mobilities respectively. It is important to note that the value of capacitance does not depend on the built-in voltage but the light intensity through the rate of generation G. Here, the capacitance-voltage measurement taken is the total impendence of the device at a certain frequency.

The Motty-Schottky analysis that was employed to determine the doping concentration from capacitance-voltage measurements is shown in Fig. 8. The curve describes the reciprocal of the square of capacitance $(1/c^2)$ versus the potential difference.
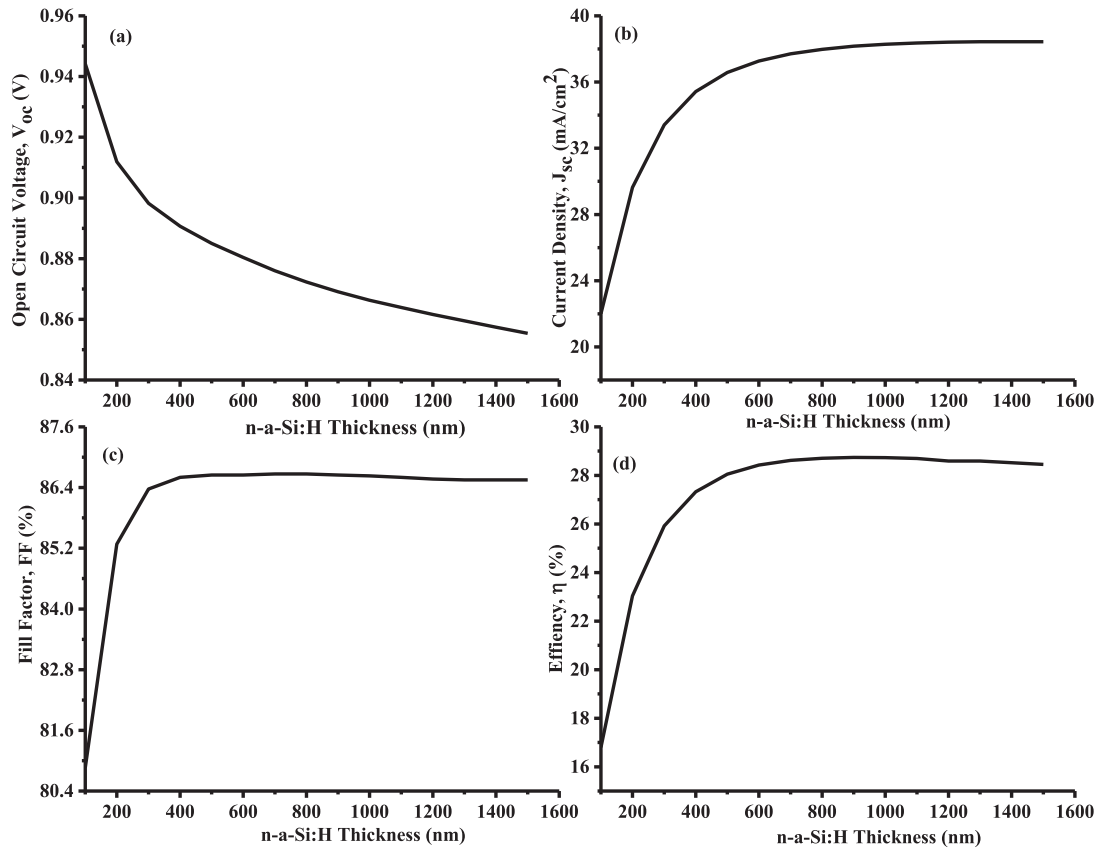
Fig. 5. (a) Open-circuit and current density (b) current density, (c) fill factor and (d) efficiency as functions of n-a-Si:H thickness. (For interpretation of the references to color in this figure legend, the reader is referred to the web version of this article.)
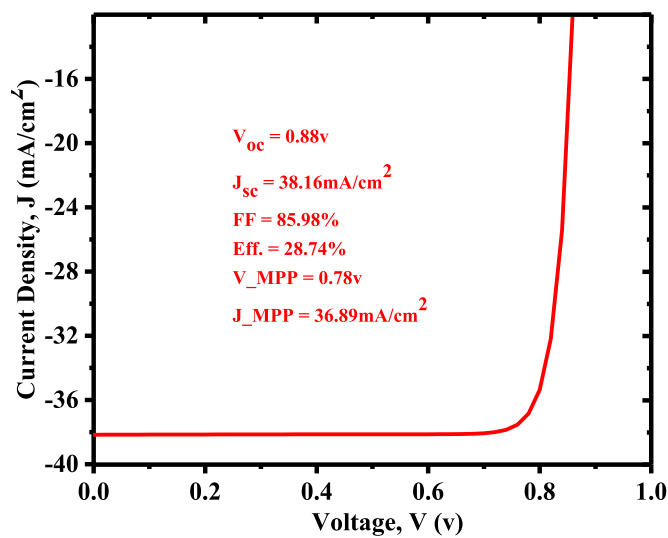
Fig. 6. J-V characteristics of the solar cell. (For interpretation of the references to color in this figure legend, the reader is referred to the web version of this article.)
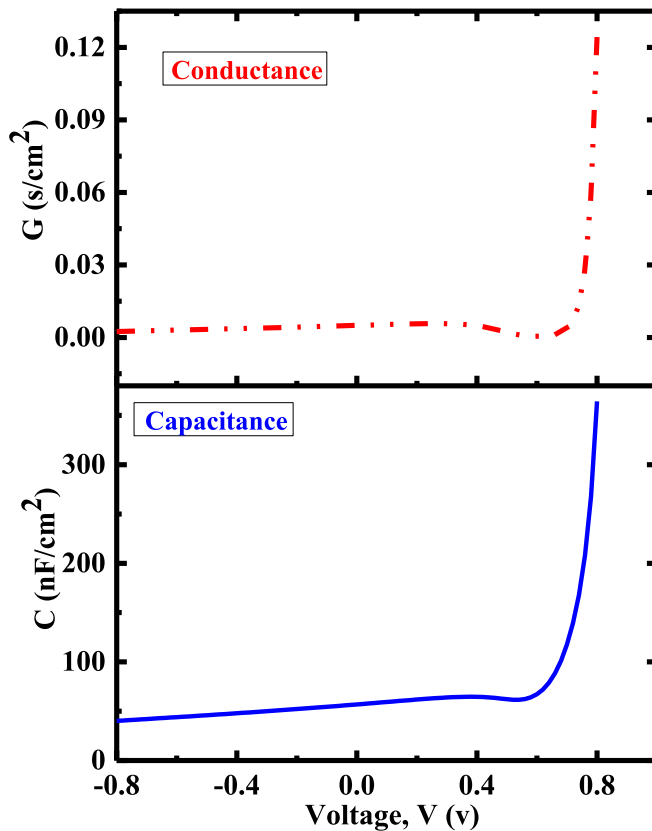
Fig. 7. Capacitance and conductance curves as a function of voltage of FTO/TiO2/n-a-Si:H/ i-a-Si:H/ p-a-Si:H/*p*+-BSF Silicon solar cell. (For interpretation of the references to color in this figure legend, the reader is referred to the web version of this article.)
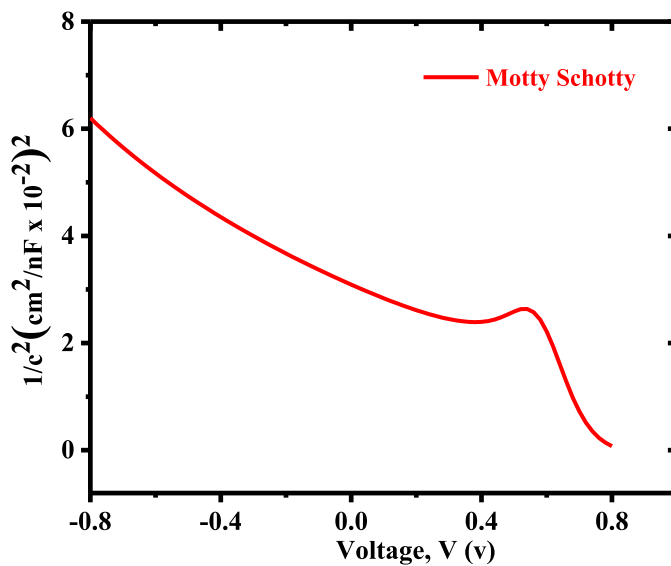
Fig. 8. Motty-Schottky curves as a function of voltage of FTO/TiO2/n-a-Si:H/ i-a-Si:H/ p-a-Si:H/*p*+-BSF Silicon solar cell. (For interpretation of the references to color in this figure legend, the reader is referred to the web version of this article.)

Conclusion

FTO/TiO$_2$ multilayer thin films were successfully simulated using MATLAB software using *n* and *k* values of FTO and TiO$_2$ extracted from the literature. The simulations showed that the FTO (100 nm)/TiO$_2$(5 nm) multilayer combination had optimum transmittance with average transmittance and reflectance of 0.82 and 0.33 respectively in wavelength range 380–780 nm. These multilayer thin films indicated very low absorption in the region 560 nm-877 nm, which was almost zero, meaning that at this region, the transmittance is very high and the films have very low reflectance, which, in turn, means that with these multilayer thin films, the reflectance losses in silicon heterojunction solar cells are minimized, hence leading to improved power conversion efficiency of silicon solar cell up to 28.74%.

Declaration of Competing Interest

The authors have no conflicts of interest.
To the best of our knowledge, none of the authors have any conflict of interest, financial or otherwise.

Acknowledgement

Appendix

Appendix 1

MATLAB code for simulation of FTO/TiO$_2$ multilayer on glass substate.

```
% Load n & k datafiles other materials
load glass_rubin.txt, load tio2_palik.txt, load pk.txt, load tio2_p.txt;
load air.txt, load FTO.txt.TXT, load diel_1_5.txt, load tio2_p.txt, load FTO_m.txt;
load N.txt, load N1.txt, load N2.txt, load N3.txt, load N4.txt, load N5.txt, load N6.txt;
%choose substrate
sub=diel_1_5;
%1. Choose wavelength interval & layers: (you can add more layers and have layers on both sides)
lambda=300:5:2500; L=length(lambda); l1= FTO.txt; l2=tio2_p; l3=air; l4=air; l5=air; l6=air; l7=air; l8=air; l9=air;
for i = 2:3% Interpolate to lambda steplength
subint(:,i)=interp1(sub(:,1),sub(:,i),lambda(:)); l1int(:,i)=interp1(l1(:,1),l1(:,i),lambda(:));
l2int(:,i)=interp1(l2(:,1),l2(:,i),lambda(:)); l3int(:,i)=interp1(l3(:,1),l3(:,i),lambda(:));
l4int(:,i)=interp1(l4(:,1),l4(:,i),lambda(:)); l5int(:,i)=interp1(l5(:,1),l5(:,i),lambda(:));
l6int(:,i)=interp1(l6(:,1),l6(:,i),lambda(:));
End
%2. Define your structure.
%2.1 Specify thicknesses of each layer in nm.
d9=0; d8=0; d7=0; d6=0; d5=0; d4=0; d3=0; d2=5; d1=200; d_s=1000000;
% d_s=substrate thickness, d1=film 1 thickness, etc.
thickness= [d8 d7 d6 d5 d4 d3 d2 d1 d_s]; thickness back= [d_s d1 d2 d3 d4 d5 d6];
%2.2 Specify whether the layers are coherent (1) or not (0)
c6=1; c5=1; c4=1; c3=1; c2=1; c1=1; c_s=0;
coherence= [c6 c5 c4 c3 c2 c1 c_s]; coherence_back= [c_s c1 c2 c3 c4 c5 c6];
%2.2 Give (read or calculate) N=n+ik for each layer.
n6=(l6int(:,2)+j*l6int(:,3))'; n5=(l5int(:,2)+j*l5int(:,3))'; n4=(l4int(:,2)+j*l4int(:,3))'; n3=(l3int(:,2)+j*l3int(:,3))'; n2=(l2int(:,2)+j*l2int(:,3))';
   n1=(l1int(:,2)+j*0.95*l1int(:,3))'; n_s=(subint(:,2)+j*subint(:,3))';
N_data= [n6; n5; n4; n3; n2; n1; n_s;]; N_data_back= [n_s; n1; n2; n3; n4; n5; n6;];
N_in=ones (1, L); N_out=ones (1, L);
n1 =n1';
%2.3 Give the angle of incidence
theta_in=0*pi/180;
%3. Calculate R and T with RT_calc
[R_t,T_t,R_p,R_s,T_p,T_s,theta_out, theta,S_p,S_s]=RT_calc(theta_in,lambda,N_data,thickness,coherence,N_in,N_out);
[R_tb,T_tb,R_pb,R_sb,T_pb,T_sb,theta_outb, thetab,S_pb,S_sb]=RT_calc(theta_in,lambda,N_data_back,thickness_back,coherence_back,N_in,N_out);
%hold on; plot(lambda,R_s,lambda,T_s);% Plot spectrum
%hold on; plot (lambda,T_t,'r', lambda,R_t,'r')%lambda,R_tb);% Plot spectrum
T_t = T_t';
R_t = R_t';
```

Appendix 1 (*continued*)

```
A = 1-(T_t+R_t);%gives absorption
BG = [T_t R_t];%gives R and T in column form
n = real(n1);
k = imag(n1);
Q = [n k];
xlim[300 900];
plot(lambda,T_t,'r')
hold on
plot(lambda,R_t,'b')
hold off
```

Supplementary materials

Supplementary material associated with this article can be found, in the online version, at doi:10.1016/j.sciaf.2023.e01678.

References

[1] D. Antoine, F. Antonin, A. L, L Levrat, Silicon heterojunction solar cells: towards low-cost high-efficiency industrial devices and application to low-concentration PV, Energy Procedia 77 (2015) 508–514.

[2] A. Goebtzberger, V. Hoffman, Photovoltaic Solar Energy Generation, Springer, New York, 2005.

[3] R. Crandall, Photocapacitance of mobile carriers in hydrogenated amorphous silicon solar cells, Appl. Phys. Lett. (1983) 451–453.

[4] F. Zhiyong, L. Qingfeng, Reducing reflection losses in solar cell, SPIE:Newsroom (2014) 1–4.

[5] H. Masahiko, O. Yoshihiro, O. Kousuke, S. Jun-ichi, Reduction in connecting resistivity and optical reflection loss at intermediate layer for mechanically stacked multijunction solar cells, Jpn. J. Appl. Phys. 57 (2018) 1–5.

[6] M. Saïdou, K. Mohamadou, G Sissoko, Silicon Solar Cells: Recombination and Electrical Parameters, 2010 Retrieved from ISBN: 978-953-307-052-0http://www.intechopen.com/books/solar-energy/silicon-solar-cells-recombination-and-electricalparameters.

[7] C. Hirst, N.J. Ekins-Daukes, Fundamental losses in solar cells, Progress Photovol. 19 (2011) 286–293.

[8] D. Vikas, N. Surya, Anti-reflection coatings for highly efficient solar cells, Res. Gate (2015) 45–52.

[9] B. Gandham, R. Hill, H. Macleod, M. Bowden, in: Antireflection Coatings On Solar Cells, Elsevier Sequoia S.A, 1979, pp. 3–22.

[10] Zhang, Effect of copper evolution on photoelectric properties of ZnO/Cu/ZnO hybrids, Appl. Phys. A (2019) 1–9.

[11] J. Wanga, D. Shi, Spectral selective and photothermal nano structured thin films for energy efficient windows, Appl. Energy 208 (2017) 83–96.

[12] M. Burgelman, P. Nollet, S. Degrav, Modelling polycrystalline semiconductor solar cells, Thin Solid Films 361 (362) (2000) 527–532.

[13] A. Langenbucher, Law of Refraction (Snell's Law), Springer, Berling, 2018.

[14] I. DIN 1349 Blatt, Durchgang Optischer Strahlen Durch Medien, Beuth-Verriebs Gmbh, Berlin, 1972.

[15] M. Mghendi, E. Wäckelgård, A. Roos, Preparation and characterization of solar selective SnOx:f coated aluminum reflector surfaces, Thin Solid Films 374 (1) (2000) 1–9.

[16] T. Paulick, Inversion of normal-incidence (R,T) measurements to obtain n+ik for thin films, Appl. Opt. 25 (1986) 562–564.

[17] P. Pfrommer, J. Lomas, C. Seal, C. Kupke, The radiation transfer coated and tinted glazing, Sol. Energy 54 (5) (1995) 287–299.

[18] H. Movla, Optimization of CIGS based thin film solar cells:numerical simulation and analysis, Optik (Stuttg) (2014) 67–70.

[19] F. Hossain, M. Faisal, H. Okada, Device modeling and performance analysis of perovskite solar cells based on similarity with inorganic thin film solar cells structure, in: Electrical, Computer & Telecommunication Engineering (ICECTE), IEEE, Bangladesh, 2016, pp. 1–4.

[20] A. Husainat, W. Ali, P. Cofie, J. Attia, J. Fuller, Simulation and analysis of methylammonium lead iodide (CH3NH3PbI3) perovskite solar cell with Au contact using SCAPS 1D simulator, Am. J. Opt. Photon. 7 (2) (2019) 33.

[21] A. Md. Feroz, H. Md. Faruk, Influence of Front and Back Contacts on Photovoltaic Performances of p-n Homojunction Si Solar Cell: considering an electron-blocking layer, Int. J. Photoenergy (2017) 1–6, doi:10.1155/2017/7415851.

[22] V. Odari, R. Musembi, J. Mwambora, Device simulation of Sb2S3 Solar cells by SCAPS-1D Software, Afr. J. Phys. Sci. 3 (2019) 39–54.

[23] N. Selmane, A. Checknane, S. Hilal, Optimization of Al-doped ZnO transparent conducting oxide and emitter layers for enhanced performance of Si heterojunction solar cells, J. Electron Mater. (2020) 1–12.

[24] C. Granqvist, Transparent conductors as solar energy materials: a panoramic review, Sol. Energy Mater. Sol. Cells (2007) 1529–1598.

[25] J. Shadia, N. Riyad, Effect of processing on the electrical properties of spray-deposited SnO2:F thin films, J. Appl. Sci. (2008) 672–677.

[26] A. Kaur, Mitra, K Yadav, Pulsed laser deposited Al-doped ZnO thin films for optical applications, Progr. Nat. Sci. (2015).

[27] K. Bittkau, T. Kirchatz, U. Rau, Optical design of spectrally selective interlayers for perovskite/silicon heterojunction tandem solar cells, Opt. Express 26 (18) (2018) 1–12.

[28] W. Isoe, M. Mageto, M. Maghanga, M. Mwamburi, V. Odari, C. Awino, Thickness dependence of window layer on CH3NH3PbI3-XClX perovskite solar cell, Hindawi Int. J. Photoenergy (2020) 1–7, doi:10.1155/2020/8877744.